A Fast-Charging Switching-Based Charger With Adaptive Hybrid Duty Cycle Control for Multiple Batteries

Pang-Jung Liu, *Member, IEEE*, and Chia-Hung Yen

***Abstract*—To reduce circuit complexity and better control the charging current for parallel charging, a switching-based charger with an adaptive hybrid duty cycle control (AHDCC) for multiple batteries is presented. Depending on the voltage difference of the batteries, the AHDCC mechanism automatically delivers a different amount of energy to each battery to realize battery voltage balance and reduce power losses. Since an intermittent charging method is adopted in the constant current (CC) mode, the effect of voltage drop across the battery's parasitic resistor can be removed, and thus the charging time in CC mode is prolonged. AHDCC adjusts the charging current, prolongs the charging period in CC mode, and entirely turns on the auxiliary switches in the constant voltage mode. As a result, the functionalities of fast charging and battery voltage balance can be realized concurrently. The experimental results demonstrate that the peak efficiency of the charger is up to 89.4% and the total charging time of two batteries is slightly smaller than that of a single battery.**

***Index Terms*—Charger, constant current (CC) mode, constant voltage mode, fast charging.**

I. Introduction

NOWADAYS, battery-powered portable electronic devices such as smartphones, tablets, and multimedia entertainment devices have become popular and ubiquitous. A secondary battery plays an important and necessary role as a power source for those portable gadgets. Among secondary batteries, the Lithium-ion (Li-ion) battery is a popular choice due to its small size, lightweight, high energy density, and low self-discharge [1]–[3].

Generally speaking, the charging procedure of a Li-ion battery can be divided into three charging modes, including trickle current (TC) mode, constant-current (CC) mode, and constant-voltage (CV) mode as illustrated in Fig. 1 [4]–[7]. Since the internal resistance of a Li-ion battery is high when the battery is discharged deeply, TC mode is needed to prevent the battery from being damaged under a small charging current [2], [4]. Once the battery voltage is larger than voltage V_L, the internal resistance of a Li-ion battery becomes low, so the charging procedure is changed from TC mode to CC mode. CC mode is the main charging procedure when using a large charging current. When the battery voltage approaches voltage V_H, the charging procedure enters CV mode. In CV mode, the charging current should be progressively reduced to allow the battery to slowly accomplish the rated voltage and to avoid overcharging. Once charging current is less than current $I_{\rm end}$, the charging procedure is ended.

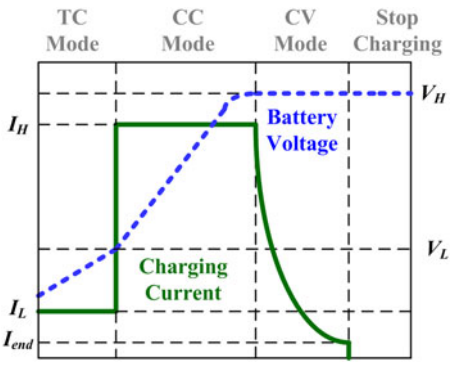

Fig. 1. Li-ion battery charging procedure.

It is convenient for a battery charger to allow multiple batteries to be charged simultaneously [8]–[11]. One architecture is to use multiple power converters connected in parallel for concurrent charging as shown in Fig. 2(a). Each power converter can be controlled independently, so the charging procedure for each battery can be chosen flexibly. However, the number of components used such as switches, inductors, and capacitors increases with the multiple. Furthermore, the production cost and circuit board area on the printed circuit board (PCB) will be significantly larger.

To reduce circuit complexity and production cost, one power converter is used to charge multiple batteries altogether as shown in Fig. 2(b). The two diodes D_1 and D_2 are adopted to avoid circulating current between the two batteries. When the converter operates in TC or CC mode, the value of the output current $I_{\rm o}$ can be controlled well, but the values of currents I_1 and I_2 through the two batteries depend on the characteristics of the batteries and diodes. For instance, when the forward voltage of D_1 is larger than that of D_2 and the open-circuit voltage V_{BO1} is larger than voltage V_{BO2}, D_1 and D_2 are prone to be turned off and on, respectively. Hence, I_1 becomes zero and I_2 is equal to I_o. On the other hand, when D_1 and D_2 conduct, I_1 and I_2 share current I_o. It is clear that although I_o is regulated, I_1 and I_2 cannot

Manuscript received November 30, 2015; revised February 27, 2016; accepted April 13, 2016. Date of publication April 21, 2016; date of current version December 9, 2016. This work was supported in part by the Ministry of Science and Technology, Taiwan, under Grant MOST 103-2221-E-027-131 and 104-2221-E-027-129. Recommended for publication by Associate Editor M. Ferdowsi.

The authors are with the Department of Electrical Engineering, National Taipei University of Technology, Taipei 10608, Taiwan (e-mail: pjliu@ntut.edu.tw; tiger.gree@gmail.com).

Color versions of one or more of the figures in this paper are available online at http://ieeexplore.ieee.org.

Digital Object Identifier 10.1109/TPEL.2016.2555998

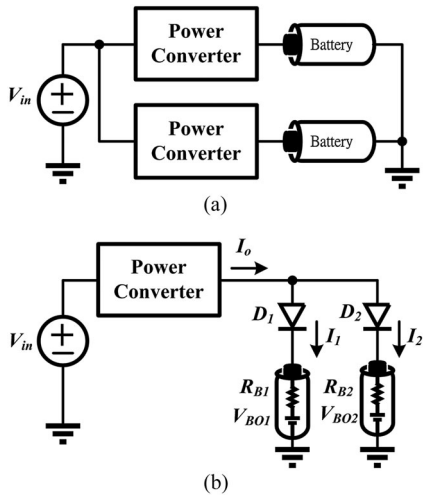

Fig. 2. (a) Multiple power converters and (b) single power converter for charging multiple batteries.

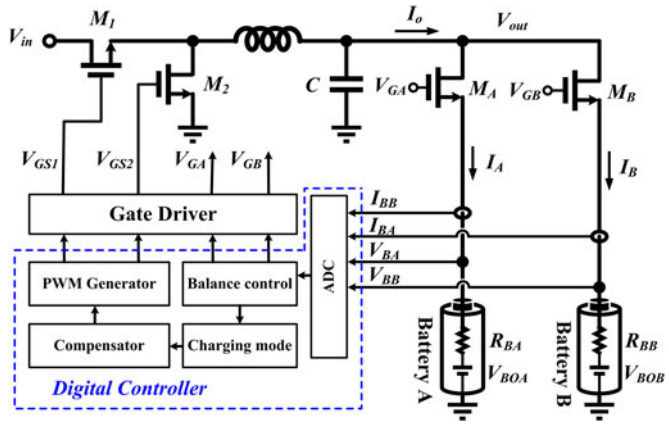

Fig. 3. Proposed switching-based charger with AHDCC.

TABLE I
THREE OPERATING MODES OF THE SWITCHING-BASED CHARGER WITH THE AHDCC METHOD

Battery voltage	Charging process	State of auxiliary switches	Charging state
$<V_{\mathrm{L}}$	TC mode	Alternatively on and off	Fixed low charging current
$>V_{\mathrm{L}}$ and $<V_{\mathrm{H}}$	CC mode	Alternatively on and off	Varying large charging current
$>V_{\mathrm{H}}$	CV mode	Always on	Constant voltage

be controlled well. In the beginning of the charging procedure, one battery with a low voltage is prone to be charged with an uncontrolled large current. Since in the worst case the maximum battery current is equal to I_o, the maximum I_o value should be set to the standard value according to the battery datasheet to prevent battery damage. However, in the balance case, the battery current becomes $0.5I_o$, and thus the charging time will be prolonged significantly. Furthermore, the efficiency of the charger with diodes decreases dramatically when the charger operates with a large charging current or low output voltage.

Once one of the battery voltages reaches the predefined voltage V_H, the operating procedure is switched from CC mode to CV mode. During the charging procedure, the battery voltage is the summation of the open-circuit voltage V_{BO} and the voltage across the parasitic resistor R_B including contact resistance, PCB wire trace resistance and battery cell resistance in series. Owing to the R_B effect, premature transition will cause the charging current to decrease dramatically, and thus the charging time of the battery with a low energy will be prolonged. Contrarily, delayed transition will cause the battery voltage to be too high because of the large charging current, resulting in battery damage [6], [12]. This issue of determining a proper transition point will be worsened when a single power converter charges the multiple batteries simultaneously.

In order to reduce circuit complexity and better control the charging current for parallel charging, a switching-based charger with an adaptive hybrid duty cycle control (AHDCC) for multiple batteries is presented in this paper. AHDCC is designed to deliver different amounts of energy to multiple batteries to achieve battery voltage balance. AHDCC adjusts the charging current, adopts an intermittent charging method in CC mode, and fully turns on the auxiliary switches in CV mode to realize fast and safe charging. In Section II, the proposed switching-based charger with AHDCC is addressed. Section III introduces the digital controller design. Finally, experimental results and conclusions are drawn in Sections IV and V, respectively.

II. DESIGN PROPOSED SWITCHING-BASED CHARGER WITH AHDCC

A simple switching-based charger with the AHDCC shown in Fig. 3 is presented to achieve the functionalities of fast charging and battery voltage balance for parallel charging. Compared with Fig. 2(b), two auxiliary switches M_A and M_B are employed to reduce conduction losses and enable flexible selection of the charging methods. However, a circulating current will be produced when the voltage difference between the two batteries is large enough to turn on the body diode of one auxiliary switch while the other auxiliary switch is also turned on. To prevent circulating current and transfer power between the two batteries, the battery with high energy can be discharged with pulse discharging method to the other battery and the output capacitor, before the charging procedure. Three operating modes of the switching-based charger with AHDCC method are summarized in Table I. More detailed information will be explained as follows.

A. Adaptive Duty Cycle and Varying Charging Current Control

When the proposed charger operates in TC and CC modes, switches M_A and M_B are alternatively turned on and off as shown in Fig. 4. The sum of the conduction duration of M_A and M_B is equal to the period T_p ($i.e.,\ T_p = T_1 + T_2$). When M_A is on and M_B is off, output current I_o charges battery *A*. Alternatively, battery *B* is charged by I_o when M_A is off and M_B is on. With such an arrangement, the power converter is always active and the input power can be fully utilized because

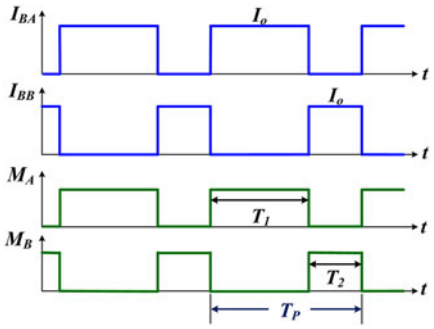

Fig. 4. Illustration of the intermittent charging strategy when the power converter operates in TC and CC modes.

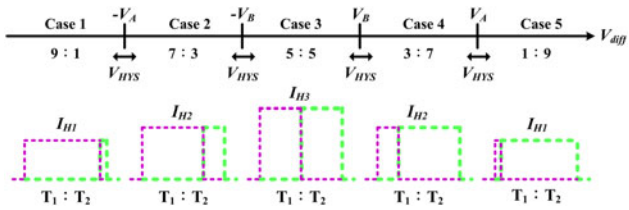

Fig. 5. Concept of the adaptive duty cycle and varying charging current control in CC mode.

each battery is able to share some amount of the current at once. One battery is charged with a constant current when switched on while the other battery is at rest when switched off. This type of charging scheme for the batteries is commonly known as intermittent charging or pulse charging [13]–[19]. The intermittent mechanism supplies a rest period for the electrolyte's ions to diffuse and also distributes the ions more uniformly, so the battery life cycle can be prolonged.

When M_A or M_B is turned on, the output voltage $V_{\rm out}$ can be expressed, respectively, as

$$V_{{\rm out},A} = V_{BOA} + (R_{BA} + R_{onA})\, I_A \quad \text{when } M_A \text{ is on and } M_B \text{ is off} \tag{1}$$

$$V_{{\rm out},B} = V_{BOB} + (R_{BB} + R_{onB})\, I_B \quad \text{when } M_B \text{ is on and } M_A \text{ is off} \tag{2}$$

Subscripts *A* and *B* represent the branches of battery *A* and *B*, respectively. V_B is the battery voltage including the open-circuit voltage V_{BO} and a voltage drop across the parasitic resistor R_B. $R_{\rm on}$ is the on-resistance of the auxiliary switch. Since the parameters V_{BO}, R_B, and $R_{\rm on}$ are not identical for the two branches, $V_{{\rm out},A}$ and $V_{{\rm out},B}$ are unequal. In other words, the output voltage $V_{\rm out}$ will be ringing corresponding to period T_p. The power losses of the charger increase when $V_{\rm out}$ is charged and discharged periodically. To alleviate this issue, the battery voltages should be kept the same. Hence, the conduction duration of the auxiliary switches M_A and M_B is adjusted dynamically based on the voltage difference $V_{\rm diff}$ of the batteries as illustrated in Fig. 5, where $V_{\rm diff} = V_{BA} - V_{BB}$. According to the four values V_A and V_B, the $V_{\rm diff}$ range is divided into five states, where V_A and V_B are set to 160 and 10 mV, respectively. Each state has a different charging duty ratio α of T_1 to T_2 and a different charging current. The voltage $V_{\rm HYS}$ represents the hysteresis range to reduce changes in the operating-state frequency. For example, when voltage $V_{\rm diff}$ is smaller than $(-V_A - V_{\rm HYS}/2)$, the charger operates in case-1 state, and the charging duty ratio α is set to 9. Since battery *A* gets more energy from the power converter, $V_{\rm diff}$ will be increased. Once $V_{\rm diff}$ is larger than $(-V_A + V_{\rm HYS}/2)$, the charger enters case-2 state. Similarly, when $V_{\rm diff}$ is larger than $-(V_B + V_{\rm HYS}/2)$, α is set to 1, which indicates that the voltages of the two batteries are almost the same. Likewise, when V_{BA} is larger than V_{BB}, the charging duty ratio α is less than 1. Moreover, to take the rest period into consideration, the average charging current passing through each battery is less than I_o when the power converter operates in CC mode. To reduce charging time and prevent battery damage, the average charging current through a battery in CC mode is increased to 1 C (the standard charging current of 1 C is suggested by the battery datasheet [20]). Therefore, the values of currents $I_{\rm H1}$, $I_{\rm H2}$, and $I_{\rm H3}$ are 1.11, 1.43, and 2 C, respectively. However, when the charging procedure operates in TC mode, the charging current is always kept constant at 0.1 C.

B. Appropriate Transition Timing Control

During the charging period, the sensed battery voltage includes voltage V_{BO} and the voltage drop across R_B. Due to the R_B effect, the transition timing from CC mode to CV mode may be too early or too late. If the mode transition happens too early, the charging time of the battery will be prolonged. On the other hand, if mode transition happens too late, the battery may suffer from overcharging. Thanks to the intermittent charging scheme, one of the battery open-circuit voltages can be sensed while $M_{\rm A}$ or $M_{\rm B}$ is tuned off, so a transition timing of each battery switching from CC mode to CV mode can be determined appropriately.

C. CV Mode Control

Since the charging time of CV mode occupies a significant portion of the total charging time [21], switches M_A and M_B are entirely turned on after the two batteries enter into CV mode. In CV mode, the output voltage $V_{\rm out}$ is fixed and V_{BO} still increases slowly, so the charging current $I_{\rm o}$ is reduced continuously. When the charging current of each battery is less than the predefined value $I_{\rm end}$, its auxiliary switch M_A or M_B will be turned off. Hence, we can avoid overcharging the batteries and the total charging time can be reduced significantly.

III. Digital Controller Design

In this work, a DSP TMS320F28035 is adopted to realize the proposed AHDCC method for the charger studied. The control flowchart of the battery-charging scheme and frequency compensation will be described and discussed as follows.

A. Flowchart of AHDCC

The main program of AHDCC is shown in Fig. 6(a), which includes parameters and I/O initialization, peripheral function setting, interrupt setting and charging control. The flowchart of the charging control is shown in Fig. 6(b) and is briefly

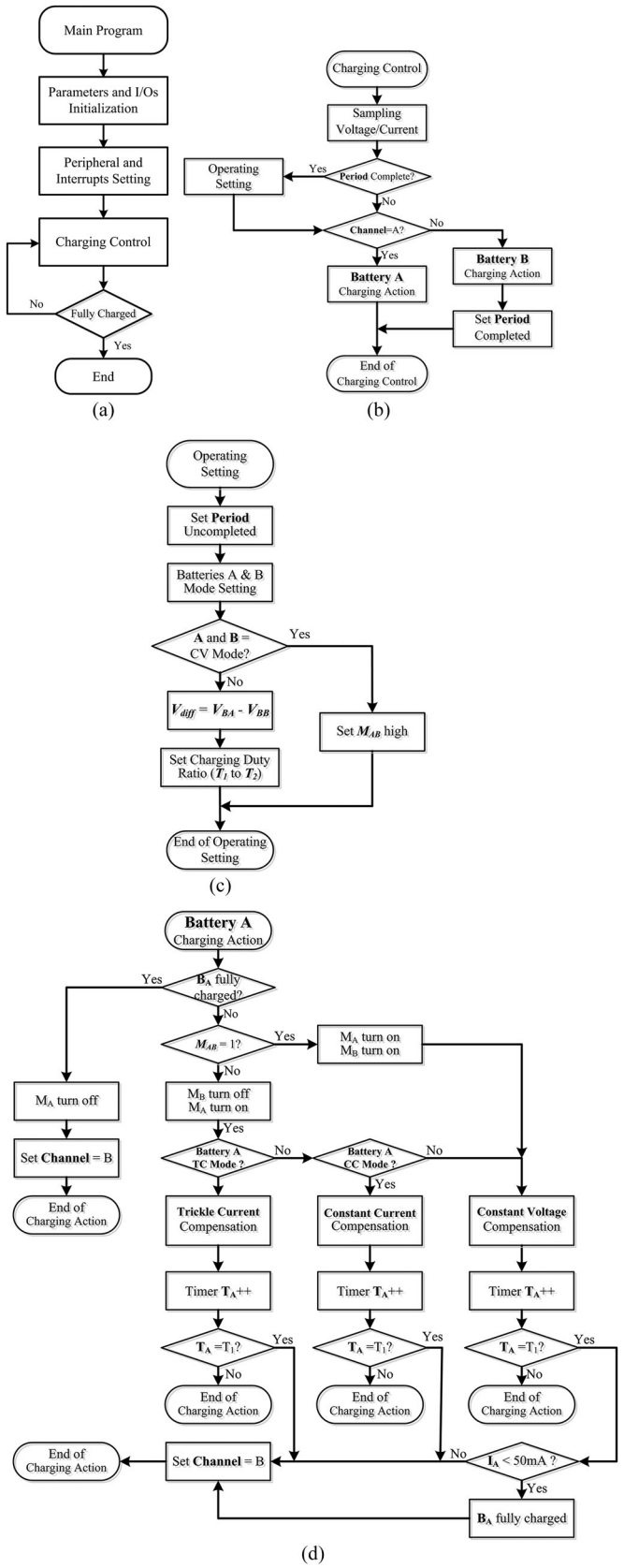

Fig. 6. Flowchart of the adaptive duty-ratio hybrid control: (a) main program, (b) charging control, (c) operating setting, and (d) charging action.

described as follows. Sampling of the battery voltage and current is performed in every switching period. As described in Section II, when battery *A* is being charged, the sensed voltage V_{BA} includes the voltage across R_{BA}. To remove the voltage drop across the parasitic resistor, the charging current I_A and voltage V_{BB} are sensed when battery *A* is being charged. Similarly, the charging current I_B and voltage V_{BA} are sensed when battery *B* is being charged. The digital controller determines whether one charging period T_p is finished or not. If so, the operating setting will be performed; otherwise, the program will enter the charging action. It should be noted that the operating setting is fulfilled for every charging period and not every switching period.

The detail of the operating setting is illustrated in Fig. 6(c). According to the value of the battery voltage, the corresponding charging mode is set. When the battery voltage is less than 3 V, TC mode is chosen. When the battery voltage is larger than 3 V and less than 4.2 V, CC mode is selected. The charging procedure enters into the CV mode when the battery voltage reaches 4.2 V. Since the charger provides a constant current to the batteries during each charging period in TC and CC modes, the charging duty ratio is determined by $V_{\rm diff}$. When both batteries operate in CV mode, the flag M_{AB} is set to high, and then switches M_A and M_B will be fully turned on for reducing the charging time.

The flowchart of the charging action of battery *A* is shown in Fig. 6(d). When battery *A* is fully charged, M_A is turned off and the flag *channel* is set to *B*. If battery *A* is not fully charged, the corresponding charging mode will be fulfilled based on the operating setting. When the charger operates in TC and CC modes, M_B and M_A are turned off and on, respectively. Then, the digital compensation is performed, and timer T_A increases by one. When the T_A value is less than T_1 determined by the operating setting, the program of charging battery *A* is ended, and in the next switching period battery *A* is still being charged. When the T_A value is equal to T_1, the flag *channel* is set to battery *B*. For the next switching period, battery *B* will start to be charged. Moreover, when the charger operates in CC mode, the charging current value is dynamically adjusted based on the corresponding charging duty ratio. Once the charging procedure of both batteries operates in CV mode, M_A and M_B are turned on entirely. If the charging current I_A is less than 50 mA, battery *A* is fully charged. Then, only battery *B* continues being charged until I_B is less than 50 mA.

B. Frequency Response

Since the proposed charger needs to operate in different modes, each mode should be analyzed separately. To analyze the frequency response of the charger, the small-signal model of the power stage is shown in Fig. 7. The battery model is composed of a constant voltage and a resistor R_B in series [22]–[23]. R_C is the equivalent resistance of the capacitor, and R_{BS} is the sum of the on resistance of the auxiliary switch and resistor R_B. $R_{\rm eq}$ includes the equivalent resistance of the inductor and switches M_1 and M_2. The control-to-output transfer functions can be derived as (3)–(4) shown at the bottom of the next page.

The block diagrams of the digital-controlled charger operating in current and voltage modes are shown in Fig. 8. The

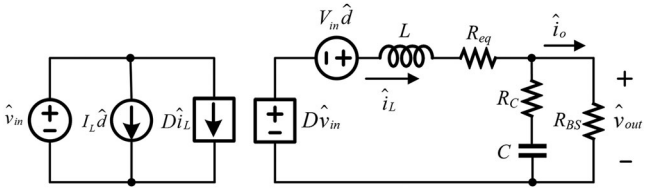

Fig. 7. Small-signal model of the charger operating in CCM.

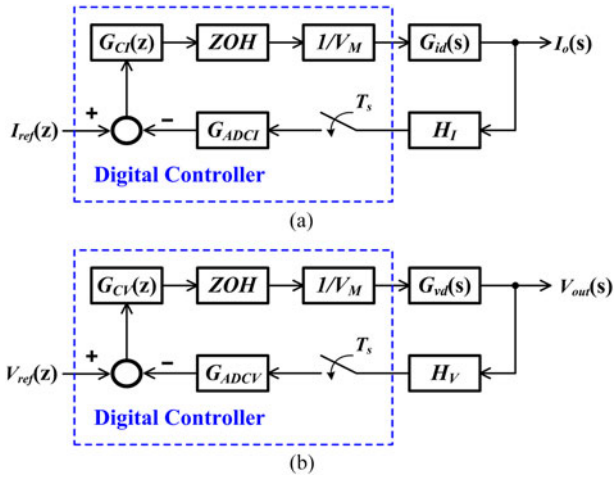

Fig. 8. Block diagram of the proposed charger for operating in (a) current and (b) voltage modes.

block diagrams include the feedback network H, A/D sampling gain G_{ADC}, the modulation gain $1/V_M$, and zero order hold ZOH, where $H_I = 1.5$, $H_V = 0.402$, $G_{ADCV} = 312.5$, $G_{ADCV} = 1242.6$, and $V_M = 1500$. Sampling frequency of the feedback output current and voltage is set to be the same as the switching frequency of the charger for synchronization. To increase the stability of the charger, the proportional-integral (PI) compensator is utilized and its z-domain equation can be derived by Tustin approximation and expressed as

$$G_C(z) = \left(\frac{K_I T_s}{2} + K_P\right)\frac{Z}{Z-1} + \left(\frac{K_I T_s}{2\,(Z-1)} - \frac{K_P}{Z-1}\right). \tag{5}$$

The Bode plots of the charger operating in current and voltage modes are shown in Fig. 9. The zero of the PI compensator is located close to the dominant pole of the power stage to perform pole-zero cancellation. The dc gain of the PI compensator determines the charger bandwidth. The two loops have approximately the same phase margin because their poles and zeros are

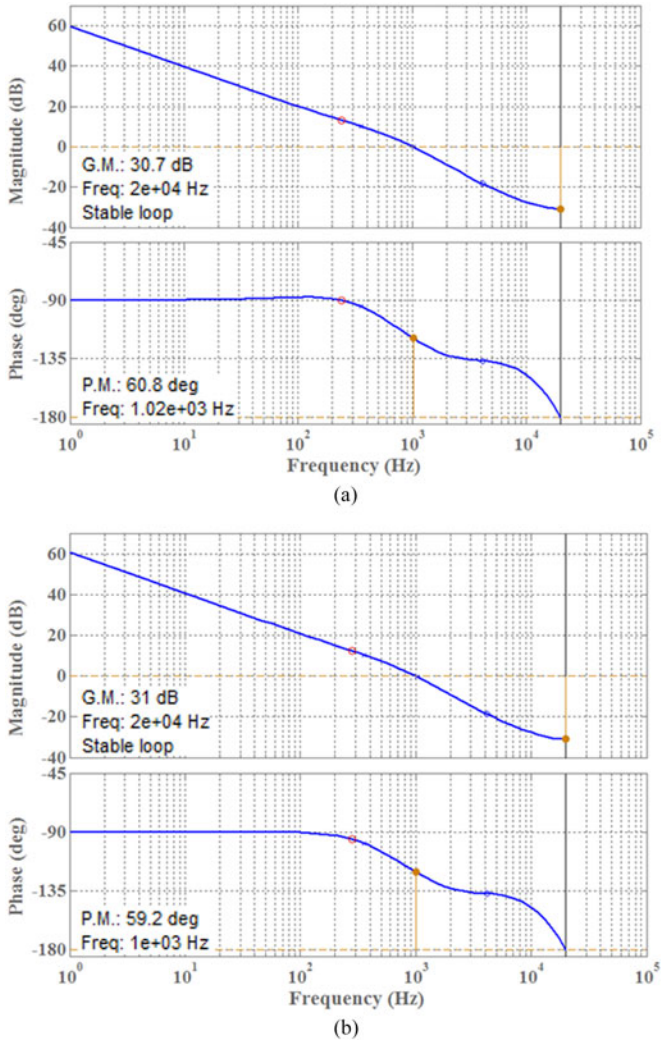

Fig. 9. Bode plots of the charger operating in (a) current mode and (b) voltage mode.

nearly at the same positions. The Bode plot results ensure the stable operation of the charger via adequate phase margin.

IV. Experimental Results

To verify the feasibility of the proposed AHDCC, a laboratory charger was implemented with an input voltage of 10–20 V, output voltage of 2.5–5 V, switching frequency of 40 kHz, charging period T_p of 1 s, and maximum output current of 1.6 A. The output inductance and capacitance were 420 μH and 47 μF,

$$G_{vd} = \frac{\widehat{v}_{\mathrm{out}}}{\widehat{d}} = V_{\mathrm{in}}\frac{sCR_CR_{BS} + R_{BS}}{s^2LC(R_C + R_{BS}) + s\left[L + CR_CR_{BS} + CR_{\mathrm{eq}}(R_C + R_{BS})\right] + R_{BS} + R_{\mathrm{eq}}}$$
$$\text{where} \quad R_{\mathrm{eq}} = R_L + DR_{M1} + (1-D)R_{M2} \tag{3}$$
$$G_{id} = \frac{\widehat{i}_o}{\widehat{d}} = V_{\mathrm{in}}\frac{sCR_C + 1}{s^2LC(R_C + R_{BS}) + s\left[L + CR_CR_{BS} + CR_{\mathrm{eq}}(R_C + R_{BS})\right] + R_{BS} + R_{\mathrm{eq}}} \tag{4}$$

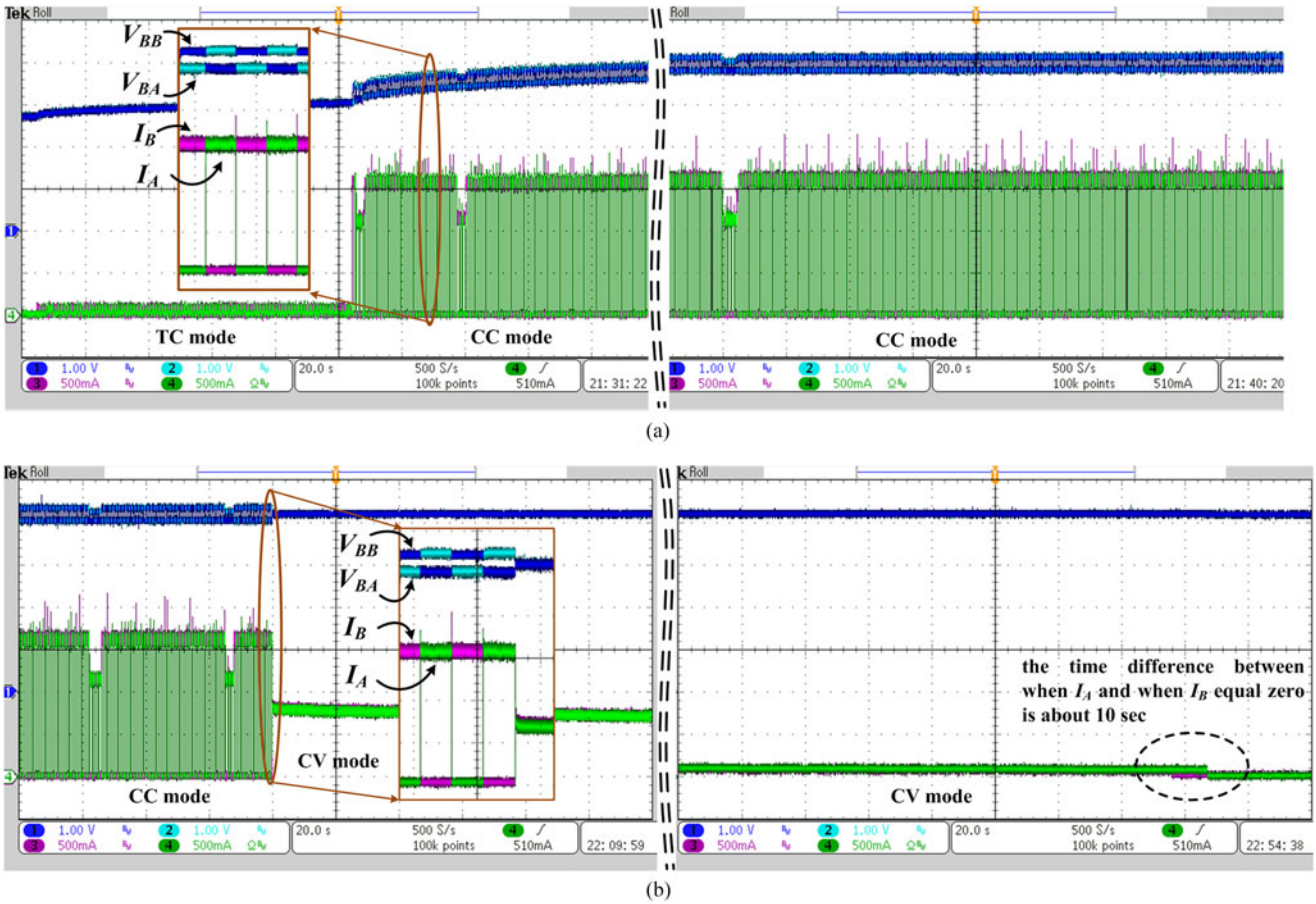

Fig. 10. Measured voltage and current waveforms of the two batteries during the charging process.

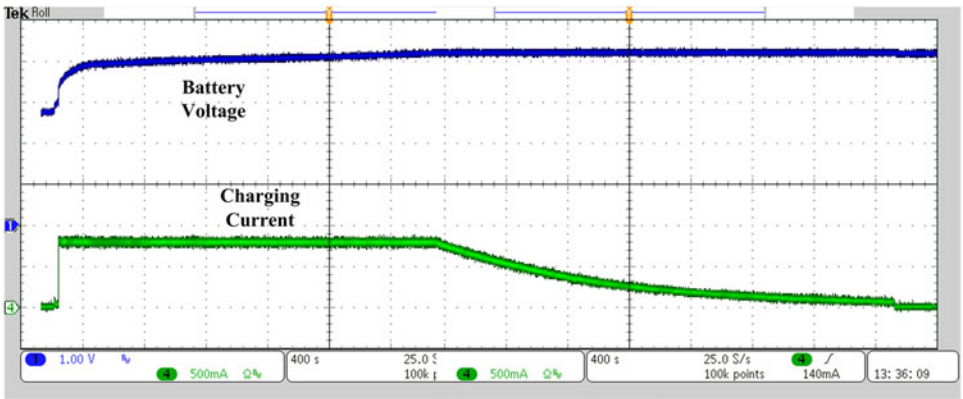

Fig. 11. Measured voltage and current waveforms of a single battery during the charging process.

respectively. Two Sanyo UR14500 (4.2 V/800 mA·h) Li-ion batteries are used as the load.

Fig. 10 shows the measured voltage and current waveforms of the two batteries during the charging process. The initial voltage of the batteries is 2.7 V, so the batteries are charged with a current of 80 mA (0.1 C) and the charging duty ratio is 50%. When the battery voltage is higher than 3 V, the charger operates in CC mode. To reduce charging time and avoid battery damage, the charging current is adjusted dynamically based on the larger charging period (T_1 or T_2). Even though the proposed charger delivers the same power to the two batteries, the incremental voltage value of the batteries is not the same because of different battery and transistor properties. Therefore, the charging duty cycle and charging current vary simultaneously when the variation of $V_{\rm dif}$ is larger than $(V_B + V_{\rm HYS}/2)$ as shown in Fig. 5. However, the voltage difference $V_{\rm dif}$ reduces quickly, so

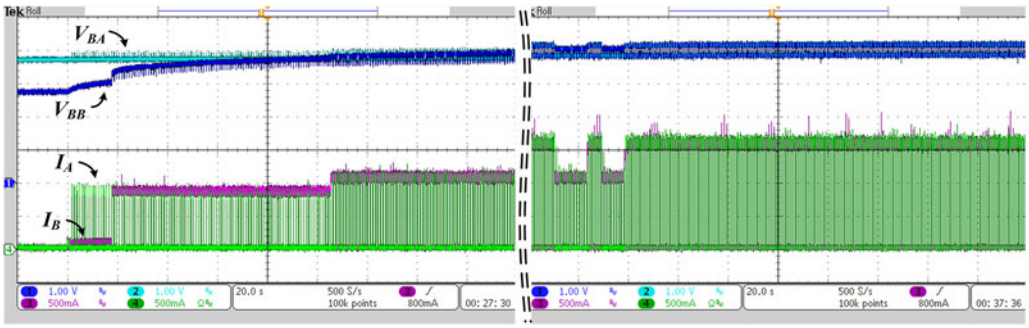

Fig. 12. Measured voltage and current waveforms of the two batteries with different initial voltages.

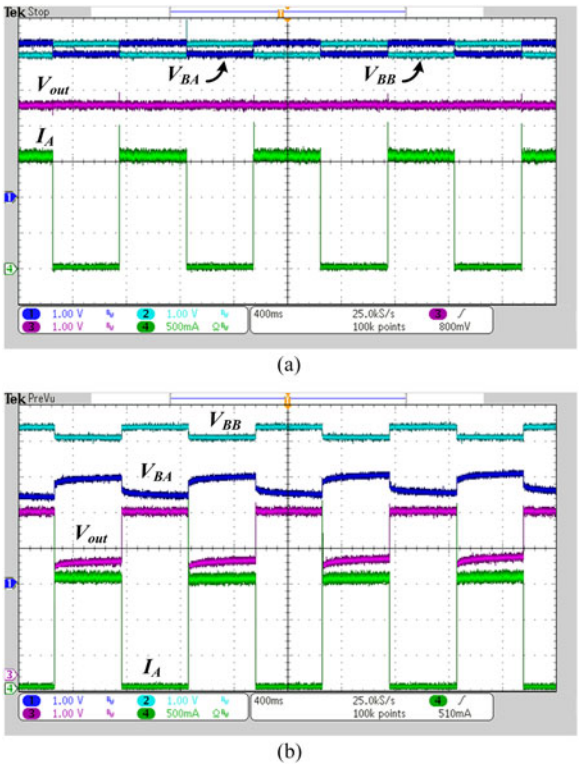

Fig. 13. Waveforms of the charger (a) with and (b) without voltage balance mechanism.

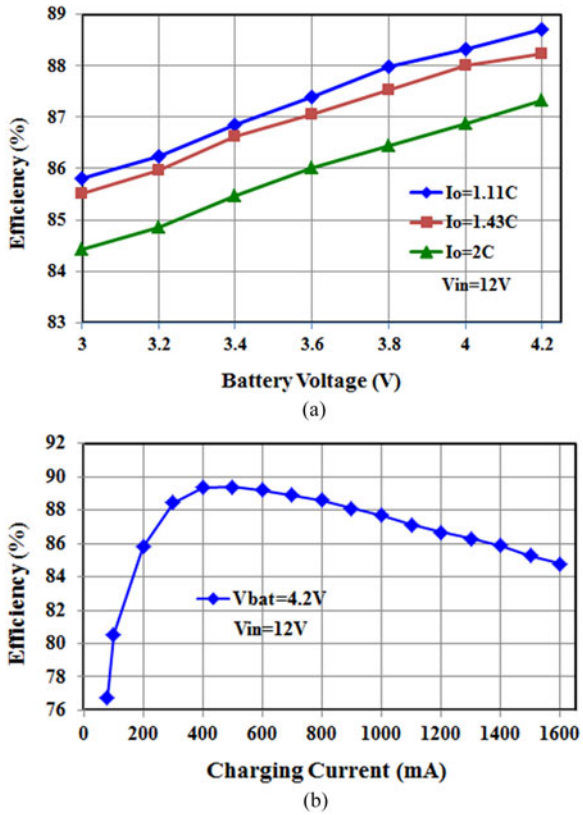

Fig. 14. Power efficiency of the charger with (a) CC and (b) CV modes.

the charging current changes to 1.6 A (2C) again. When both battery voltages approach the rated voltage, the charger provides power to the two batteries concurrently for reducing the charging time and the two charging currents are less than 800 mA (1 C). Once the battery charging current is less than 50 mA, the battery will stop charging. From Fig. 10(b), the time difference between when I_A and when I_B equal zero is about 10 s, showing that voltages V_{BA} and V_{BB} are controlled to be almost the same during the charging procedure. The total charging time is about 86 min.

Fig. 11 shows the measured voltage and current waveforms of a single battery in TC, CC, and CV charging modes. The definitions of mode changes are the same as those for two battery charging, but the total charging time is about 91 min. For charging two batteries with AHDCC, the transition timing from CC mode to CV mode can be postponed due to the removal of the battery's parasitic resistance, so the total charging time is slightly shorter than that of charging a single battery with conventional CC and CV methods.

Fig. 12 shows the voltage and current waveforms of two batteries with different initial voltages. To enlarge the difference in initial voltages and avoid circulating current between the two batteries, every battery is connected with a diode in series. One initial voltage is 2.7 V and the other is 3.7 V. Since the voltage difference $V_{\rm diff}$ is up to 1 V, 90% of the charging period belongs to the battery with lower energy, so $V_{\rm diff}$ is decreased rapidly.

$V_{\rm diff}$ is less than 154 mV after the charger operates for about 110 s, and then the charging current becomes 1144 mA (1.43 C). The total charging time is about 83 min.

Fig. 13(a) shows the waveforms of the converter with AHDCC for different initial voltage values of the two batteries. The signals from top to bottom are the two battery voltages V_{BA} and V_{BB}, output voltage $V_{\rm out}$, and charging current I_A. The cursor position of signal 3 is placed at the same level as that of signal 4. When the charger adopts AHDCC, the voltage difference between the two batteries can be diminished in a short period as shown in Fig. 12, so the output voltage is kept constant. If a charger does not have a voltage balance mechanism, the voltage difference between the two batteries is maintained as shown in Fig. 13(b). As a result, the output voltage varies according to the charging period. Moreover, the variation of the output voltage represents increasing power losses of the power converter. Fig. 14(a) illustrates the power efficiencies of the charger operating in CC mode with the input voltage of 12 V, and the three curves represent different I_o values. Fig. 14(b) shows the power efficiency of the charger operating in CV mode with the input and battery voltages of 12 and 4.2 V. The peak efficiencies of the charger in CC and CV modes are 88.7% and 89.4%, respectively.

V. Conclusion

This paper proposes a switching-based charger with the AHDCC function to reduce circuit complexity and better control the charging current for parallel charging. Based on the voltage difference of the two batteries, the AHDCC mechanism automatically determines the duty cycle of each battery. Moreover, since an intermittent charging method is adopted in CC mode, the effect of voltage drop across the battery's parasitic resistor can be removed to avoid over or under compensation in the transition voltage and to extend the charging time in CC mode. The AHDCC adjusts charging current, prolongs the charging period in CC mode, and entirely turns on the auxiliary switches in CV mode. As a result, the functionalities of fast charging and battery voltage balance can be realized concurrently. The experimental results demonstrate that the peak efficiency of the charger is up to 89.4% and the total charging time for the case of two batteries is slightly shorter than that for the case of a single battery.

Acknowledgment

The authors wish to thank National Chip Implementation Center, Taiwan, for tool training.

References

[1] L.-R. Chen, J.-J. Chen, C.-M. Ho, S.-L. Wu, and D.-T. Shieh, "Improvement of li-ion battery discharging performance by pulse and sinusoidal current strategies," *IEEE Trans. Ind. Electron.*, vol. 60, no. 12, pp. 5620–5628, Dec. 2013.

[2] B. D. Valle, C. T. Wentz, and R. Sarpeshkar, "An area and power-efficient analog li-ion battery charger circuit," *IEEE Trans. Biomed. Circuits Syst.*, vol. 5, no. 2, pp. 131–137, Apr. 2011.

[3] C.-S. Lim, K.-J. Lee, N.-J. Ku, D.-S. Hyun, and R.-Y. Kim, "A modularized equalization method based on magnetizing energy for a series-connected lithium-ion battery string," *IEEE Trans. Power Electron.*, vol. 29, no. 4, pp. 1791–1799, Apr. 2014.

[4] Y.-S. Hwang, S.-C. Wang, F.-C. Yang, and J.-J. Chen, "New compact CMOS Li-ion battery charger using charge-pump techniques for portable applications," *IEEE Trans. Circuits Syst. I, Reg. Papers*, vol. 54, no. 4, pp. 705–712, Apr. 2007.

[5] G. J. M. de Sousa, C. M. T. Cruz, C. G. C. Branco, L. D. S. Bezerra, and R. P. Torrico-Bascope, "A low cost flyback-based high power factor battery charger for UPS applications," in *Proc. IEEE Brazilian Power Electron. Conf.*, 2009, pp. 783–790.

[6] C.-H. Lin, C.-Y. Hsieh, and K.-H. Chen, "A Li-ion battery charger with smooth control circuit and built-in resistance compensator for achieving stable and fast charging," *IEEE Circuits Syst. I*, vol. 5, no. 2, pp. 131–137, Apr. 2011.

[7] R. Metidji, B. Metidji, and B. Mendil, "Design and implementation of a unity power factor fuzzy battery charger using an ultrasparse matrix rectifier," *IEEE Trans. Power Electron.*, vol. 28, no. 5, pp. 2269–2276, May 2013.

[8] V.-L. Tran and W. Choi, "Novel time division multiple control method for multiple output battery charger," *IEEE Trans. Power Electron.*, vol. 29, no. 10, pp. 1502–1505, Oct. 2014.

[9] Z. Jiang and R. A. Dougal, "Synergetic control of power converters for pulse current charging of advanced batteries from a fuel cell power source," *IEEE Trans. Power Electron.*, vol. 19, no. 4, pp. 1140–1150, Jul. 2004.

[10] J.-B. Wang and C.-Y. Chuang, "Design considerations of microprocessor-controlled multiphase battery charger with fast-charging strategy," *IET Trans. Power Electron.*, vol. 1, no. 2, pp. 143–152, Feb. 2007.

[11] F.-J. Lin, M.-S. Huang, P.-Y. Yeh, H.-C. Tsai, and C.-H. Kuan, "DSP-based probabilistic fuzzy neural network control for Li-ion battery charger," *IEEE Trans. Power Electron.*, vol. 27, no. 8, pp. 3782–3794, Aug. 2012.

[12] T.-C. Huang, R.-H. Peng, T.-W. Tsai, K.-H. Chen, and C.-L. Wey, "Fast charging and high efficiency switching-based charger with continuous built-in resistance detection and automatic energy deliver control for portable electronics," *IEEE J. Solid-State Circuit*, vol. 49, no. 7, pp. 1580–1594, Jul. 2014.

[13] H.-J. Chiu, Y.-K. Lo, C.-J. Yao, T.-P. Lee, J.-M. Wang, and J.-X. Lee, "A modular self-controlled photovoltaic charger with interintegrated circuit (I^2C) interface," *IEEE Trans. Energy Convers.*, vol. 26, no. 1, pp. 281–289, Mar. 2011.

[14] L.-R. Chen, "Design of duty-varied voltage pulse charger for improving Li-ion battery-charging response," *IEEE Trans. Ind. Electron.*, vol. 56, no. 2, pp. 480–487, Dec. 2009.

[15] S. G. Abeyratne, A. H. M. S. Abeysinghe, and D. M. R. Dissanayake, "Improvements for the pulse charger with zero current switching and isolation for electric vehicles," in *Proc. IEEE 8th Int. Conf. Ind. Inf. Syst. Conf.*, 2013, pp. 589–593.

[16] H.-J. Chiu, L.-W. Lin, P.-L. Pan, and M.-H. Tseng, "A novel rapid charger for lead-acid batteries with energy recovery," *IEEE Trans. Power Electron.*, vol. 21, no. 3, pp. 640–647, May 2006.

[17] F. Savoye, P. Venet, M. Millet, and J. Groot, "Impact of periodic current pulses on Li-ion battery performance," *IEEE Trans. Ind. Electron.*, vol. 56, no. 9, pp. 3481–3488, Sep. 2012.

[18] R. C. Cope and Y. Podrazhansky, "The art of battery charging," in *Proc. IEEE Battery Conf. Appl. Adv. Conf.*, 1999, pp. 233–235.

[19] Y. H. Liu, J. H. Teng, and Y. C. Lin, "Search for an optimal rapid charging pattern for lithium-ion batteries using ant colony system algorithm," *IEEE Trans. Ind. Electron.*, vol. 52, no. 5, pp. 1328–1336, Oct. 2005.

[20] [Online]. Available: http://www.tme.eu/ua/Document/89dd0fe7f9fb7fc9d798f4551238a5a8/ACCU-14500-0.8S.pdf, 2007

[21] S.-H. Ryu, D.-H. Kim, M.-J. Kim, J.-S. Kim, and B.-K. Lee, "Adjustable frequency–duty-cycle hybrid control strategy for full-bridge series resonant converters in electric vehicle chargers," *IEEE Trans. Ind. Electron.*, vol. 61, no. 10, pp. 5354–5362, Oct. 2014.

[22] M. Einhorn, F. V. Conte, C. Kral, and J. Fleig, "Comparison, selection, and parameterization of electrical battery models for automotive applications," *IEEE Trans. Power Electron.*, vol. 28, no. 3, pp. 1429–1437, Mar. 2013.

[23] R.-J. Wai, S.-J. Jhung, J.-J. Liaw, and Y.-R. Chang, "Intelligent optimal energy management system for hybrid power sources including fuel cell and battery," *IEEE Trans. Power Electron.*, vol. 28, no. 7, pp. 3231–3244, Jul. 2013.

Pang-Jung Liu (S'08–M'10) received the B.S. and M.S. degrees from the National Taiwan University of Science and Technology, Taipei, Taiwan, in 1998 and 2000, respectively, and the Ph.D. degree from the Graduate Institute of Electronics Engineering, National Taiwan University, Taipei, in 2010.

From 2000 to 2003, he was the Engineer at Taiwan Semiconductor Manufacturing Company. From 2003 to 2005, he was working on digital IC design with ELAN Microelectronics Corporation. From August 2010 to January 2012, he was with the Department of Electrical Engineering, National Ilan University, I-Lan, Taiwan. Since 2012, he has been with the Department of Electrical Engineering, National Taipei University of Technology, Taipei, where he is currently an Associate Professor. His research interests include power management IC, dc–dc converter, LCD/LED driver, and mixed-mode IC design.

Dr. Liu is the recipient of the Young Researcher Award in 2014 by the Ministry of Science and Technology, Taiwan.

Chia-Hung Yen was born in Changhua, Taiwan, in 1986. He received the B.S. degree from the National Changhua University of Education, Changhua, in 2009, and the M.S. degree from the National Taipei University of Technology, Taipei, Taiwan, in 2015, both in electrical engineering.

His research interests include DSP-based control system, power electronics, and the charger.